REPORT DOCUMENTATION PAGE

AFRL-SR-AR-TR-03-

0401

1. REPORT DATE (DD-MM-YYYY)	2. REPORT TYPE	3. DATES COVERED (From - To)
09-24-03	Final Technical Report	15 Jan 00 – 30 Nov 02

4. TITLE AND SUBTITLE
EPR and Optical Characterization of Photorefractive Materials Used in Agile Laser Protection

5a. CONTRACT NUMBER

5b. GRANT NUMBER
F49620-00-1-0140

5c. PROGRAM ELEMENT NUMBER

6. AUTHOR(S)
Halliburton, Larry E.

5d. PROJECT NUMBER

5e. TASK NUMBER

5f. WORK UNIT NUMBER

7. PERFORMING ORGANIZATION NAME(S) AND ADDRESS(ES)

West Virginia University Research Corp.
Office of Sponsored Programs
886 Chestnut Ridge Road
PO Box 6845, Morgantown, WV 26506

8. PERFORMING ORGANIZATION REPORT NUMBER

9. SPONSORING / MONITORING AGENCY NAME(S) AND ADDRESS(ES)

Air Force Office of Scientific Research
801 N. Randolph St. Room 732
Arlington, VA 22203-1977

10. SPONSOR/MONITOR'S ACRONYM(S)
AFOSR/NL

11. SPONSOR/MONITOR'S REPORT NUMBER(S)

12. DISTRIBUTION / AVAILABILITY STATEMENT

Distribution unlimited.

20031028 206

13. SUPPLEMENTARY NOTES

14. ABSTRACT

This is the final technical report for a project to study point defects in photorefractive crystals used in optical limiting applications. The specific materials investigated were $LiNbO_3$ and $LiTaO_3$. The experimental techniques used to characterize these crystals were optical absorption, thermoluminescence, and electron paramagnetic resonance (EPR). We obtained congruent and Mg-doped stoichiometric $LiNbO_3$ crystals from Deltronic and vapor-transport-equilibrated $LiTaO_3$ crystals from Stanford University. The stoichiometric $LiNbO_3$ crystal exhibited a large thermoluminescence peak near 94 K. There was no emission from similar congruent crystals. The thermoluminescence from the stoichiometric crystal could be excited with x-rays or 355-nm pulses from a tripled Nd:YAG laser. It is also shown that congruent $LiTaO_3$ crystals do not give thermoluminescence. However, $LiTaO_3$ crystals made stoichiometric by vapor-phase-equilibration (VTE) treatments have a large thermoluminescence peaks near 94 and 98 K. Self-trapped electrons are participating in the recombination process in both materials. The Fe^{3+} ions in the VTE-treated $LiTaO_3$ have sharp EPR lines, and a complete angular dependence set of data were collected and analyzed to obtain the g matrix and the second and fourth order crystal-field parameters.

15. SUBJECT TERMS
photorefractive materials, point defects, optical absorption, thermoluminescence, electron paramagnetic resonance, $LiNbO_3$, $LiTaO_3$

16. SECURITY CLASSIFICATION OF:			17. LIMITATION OF ABSTRACT	18. NUMBER OF PAGES	19a. NAME OF RESPONSIBLE PERSON
a. REPORT	b. ABSTRACT	c. THIS PAGE		17	Larry E. Halliburton
					19b. TELEPHONE NUMBER (include area code) 304-293-3422, ext. 1442

FINAL TECHNICAL REPORT
(For period from January 15, 2000 to November 30, 2002)

TABLE OF CONTENTS

I. Project Overview

This document is the final technical report for work performed under Air Force Office of Scientific Research (AFOSR) Grant F49620-00-1-0140. The title of the project was "EPR and Optical Characterization of Photorefractive Materials Used in Agile Laser Protection" and the Principal Investigator was Larry E. Halliburton, Physics Department, West Virginia University. In this research program, which started January 15, 2000, experimental studies were conducted to identify and characterize the point defects in $LiNbO_3$ and other photorefractive materials, such as $LiTaO_3$, that affect their performance in optical limiting applications. Both bulk and fiber samples were investigated. A primary focus was the determination of the fundamental mechanisms by which stoichiometry, impurity dopants, and native defects play a role in optical limiting. To obtain a more complete understanding of the various defect behaviors, electron paramagnetic resonance, optical absorption, and luminescence data were taken from similar samples. Work was done in conjunction with scientists at the Air Force Research Laboratory (WPAFB) in Dayton, the University of Georgia, and Stanford University.

II. Students, Publications, and Presentations

Graduate Students:

One PhD graduate student was supported during each year of this project. The majority of this support went to Madalina Chirila. A major portion of her dissertation describes results obtained during the present project. She will receive her PhD in Physics from West Virginia University in December of 2003.

Publications Citing Support from this Grant:

1. "Thermoluminescence Study of Stoichiometric $LiNbO_3$ Crystals," M. M. Chirila, N. Y. Garces, L. E. Halliburton, D. R. Evans, S. A. Basun, R. S. Meltzer, W. M. Yen, S. A. Rutkowski, D. Shumov, and J. S. Cahill, Journal of Applied Physics 92, 1221-1226 (2002).

2. "Thermally Stimulated Luminescence from Vapor-Transport-Equilibrated $LiTaO_3$ Crystals," M. M. Chirila, N. Y. Garces, L. E. Halliburton, D. R. Evans, R. K. Route, and M. M. Fejer, Journal of Applied Physics 94, 301-306 (2003).

Presentations Citing Support from this Grant:

1. "Identification and Characterization of Traps in Photorefractive Materials," L. E. Halliburton, AFOSR Photorefractive Polymer Review, San Diego, CA, July 27, 2000.

2. "Measuring the Local Temperature of Volume Gratings Written in Fe Doped $LiNbO_3$ Using Raman Spectroscopy," D. R. Evans, T. Pottenger, M. A. Saleh, S. M. Kirkpatrick, T. J. Bunning, S. Guha, N. C. Giles, and L. E. Halliburton, March Meeting of the American Physical Society, Seattle, WA, March 15, 2001.

3. "A Comparison of Point Defects in Congruent and Stoichiometric $LiNbO_3$ and $LiTaO_3$ Crystals," L. E. Halliburton, AFOSR Photorefractive Polymer Review, San Diego, CA, July 27, 2001.

III. Results from $LiNbO_3$

We obtained both undoped congruent and Mg-doped stoichiometric $LiNbO_3$ samples from Stuart Samuelson of Deltronic Crystal Industries (located in northern New Jersey). Optical absorption, thermoluminescence, and electron paramagnetic resonance (EPR) data were taken on these samples, with the major emphasis placed on the stoichiometric samples.

Figure 1 shows representative optical absorption spectra from congruent and 1% Mg stoichiometric $LiNbO_3$ crystals. These data were taken at room temperature using unpolarized light propagating along the *c* axis. The band edge shifts to higher energy as the temperature is lowered. Of even more interest, a near-edge absorption band is barely detected at room temperature, but is easily resolved at 77 K. This latter band has been assigned to a charge-transfer transition of Fe^{3+} ions (i.e., a transition in which an electron moves from an adjacent oxygen ion to the Fe ion). In congruent $LiNbO_3$ crystals, the band edge is at longer wavelengths and the charge-transfer transition of the Fe^{3+} ions is not as easily detected. Charge-transfer absorption bands have large oscillator strengths and, in the case of stoichiometric $LiNbO_3$, provide a convenient way to monitor the trace amounts of Fe^{3+} ions usually present.

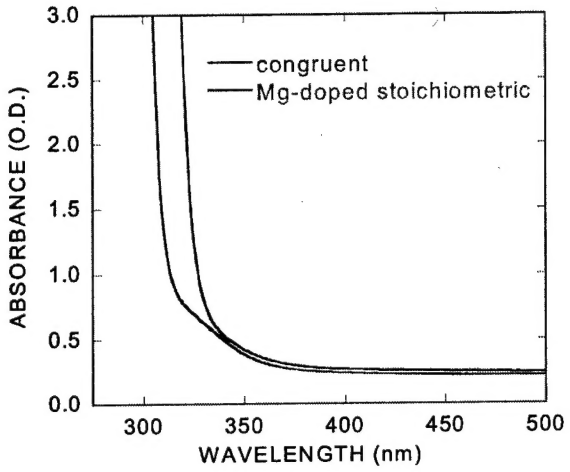

Fig. 1. Comparison of the near-edge absorption from an undoped congruent crystal and a 1% Mg stoichiometric $LiNbO_3$ crystal. An extrinsic absorption band, peaking near 320 nm and well resolved at 77 K, is attributed to trace amounts of Fe^{3+} ions.

Thermoluminescence results from a Mg-doped stoichiometric $LiNbO_3$ crystal are shown in Fig. 2. These data are presented in a three-dimensional plot with temperature, wavelength, and intensity as the axes (note that only one TL peak was observed in our samples). The results described in Fig. 2 were obtained after the sample was exposed to the pulsed 355-nm laser beam while being held at 77 K. A rapid rise in temperature then produced the observed TL. The heating rate was approximately 10.7 K/s and a complete measurement of the wavelength dependence of the emission was made every 0.9 K with the CCD spectrograph and camera. Cross-sectional views of the data in Fig. 2 are provided in Figs. 3 and 4. The temperature dependence of the emission, corresponding to a wavelength near the peak, is shown in Fig. 3. The maximum in the emission occurs near 94 K and the width of the TL peak is sharp, indicating that the release of

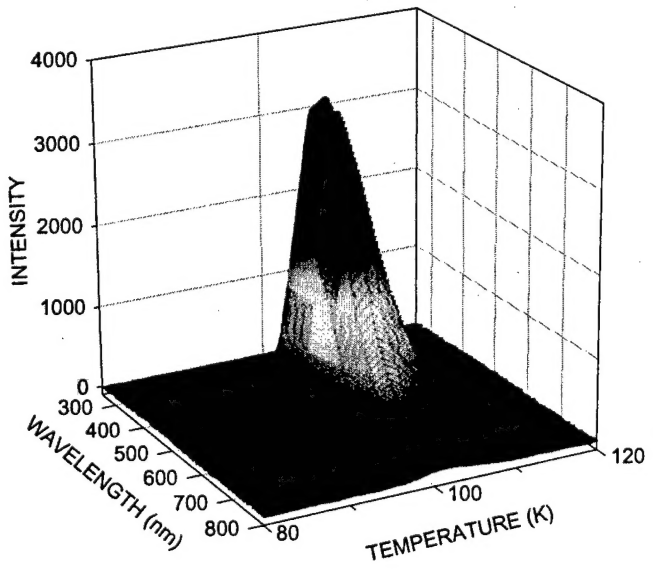

Fig. 2. Three-dimensional view of the thermoluminescence data taken from a 1% Mg stoichiometric $LiNbO_3$ crystal after excitation at 77 K with a pulsed 355-nm laser. The intensity of the emission is plotted as a function of both temperature and wavelength.

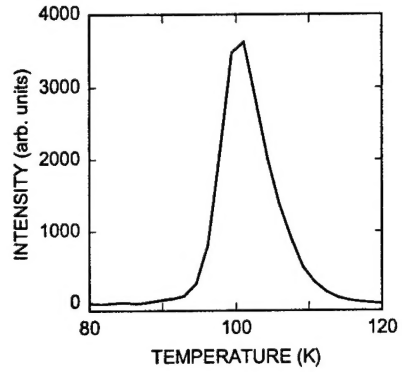

Fig. 3. A cross-section view (taken from the data in Fig. 2) showing the temperature dependence of the thermoluminescence from $LiNbO_3$. These data correspond to a wavelength of 440 nm (i.e., the maximum of the emission). The TL peak occurs near 94 K.

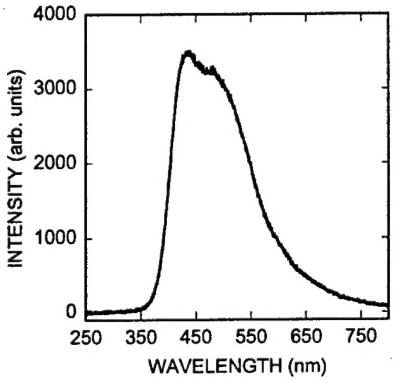

Fig. 4. A cross-section view (taken from the data in Fig. 2) showing the wavelength dependence of the thermoluminescence from $LiNbO_3$. These data correspond to a temperature of 94 K (i.e., the maximum of the emission). The TL peak occurs near 440 nm.

charge leading to radiative recombination is a well-defined and discrete phenomenon. (As an aside, we note that a slower warming rate, which is more typical in many TL experiments, would cause the peak to shift to a slightly lower temperature.) The wavelength dependence of the emission, monitored at 94 K, is shown in Fig. 4. These data have been corrected for system response, and they verify that the peak in the emission occurs near 440 nm. In addition to the 355-nm laser beam, two other excitation sources (60-kV x rays and a 325-nm laser) were used to produce the TL in our $LiNbO_3$ crystals. And, in each case, the TL results were the same as those shown in Figs. 2, 3, and 4.

Separate experiments were conducted to help identify the electron and hole centers that are participating in the radiative recombination process described by the data in Fig. 2. Optical absorption measurements were made at 10 K in the near-infrared region before and during an exposure of a 1% Mg stoichiometric $LiNbO_3$ crystal to the 325-nm laser beam and separately to the 355-nm laser beam. Similar results were observed for both wavelengths. We did not repeat

this experiment using the 60-kV x rays because of the technical problems associated with introducing these high-energy x rays into the optical cryostat. The absorption band induced by the 325-nm laser peaks near 1200 nm. This 1200-nm absorption band was initially observed in Mg-doped stoichiometric $LiNbO_3$ crystals by Sweeney *et al.* These earlier investigators suggested that it was associated with a shallow electron trap, and we extend that assignment to specifically mean an electron trapped on a niobium ion at a regular lattice site. We found, in the present study, that the 1200-nm absorption band is sensitive to bleaching light, i.e., the responsible center was easily destroyed optically when experiments to determine its thermal stability, such as repeated absorption scans at various low temperatures, were attempted. Specifically, ultraviolet laser beams or x rays produce these absorbing centers while the infrared light present in the measuring beam of the FTIR spectrometer rapidly destroys the centers. The concentration of absorbing centers at any given time depends on the rates associated with these two competing mechanisms.

Low-temperature EPR spectra were taken from one of our 1% stoichiometric $LiNbO_3$ crystals. The crystal was irradiated at 77 K with x rays and rapidly transferred into the cold helium gas flowing through the microwave cavity, then the spectra were taken at 20 K with the magnetic field along the *c* axis. Next, the conditions that produced the TL peak at 94 K (see Fig. 2) were replicated by warming the irradiated crystal to 110 K while in the microwave cavity, holding it there for 5 min, and then finally returning to 20 K where the spectra were taken (with the same spectrometer settings and the same direction of magnetic field). Similar EPR results, although with lower signal-to-noise ratios, were observed when the 1% Mg stoichiometric $LiNbO_3$ crystal was initially exposed to the 325-nm or 355-nm laser beams while being held in the microwave cavity at temperatures below 77 K. It is important to note that we did not observe EPR signals from niobium antisite defects (Nb_{Li}^{4+}) in our samples after the low-temperature irradiations with x rays or the ultraviolet lasers. In contrast, congruent $LiNbO_3$ crystals contain large concentrations of niobium ions that occupy lithium sites and provide the needed charge compensation for lithium vacancies introduced during growth; these Nb_{Li}^{5+} centers trap electrons during low-temperature x-ray irradiations and form paramagnetic Nb_{Li}^{4+} centers.

Several paramagnetic point defects contributed to the EPR spectra. There was one broad underlying signal (approximately 150 G wide and centered near 3300 G) covering the central portion of the spectrum. This broad EPR spectrum has a *g* value near 2.03 and has been assigned to a trapped-hole center, i.e., a hole trapped on an oxygen ion adjacent to a lithium vacancy. After the crystal was warmed to 110 K and then returned to 20 K, the broad trapped-hole signal had decreased to approximately 40% of its initial size. Two unidentified lines appeared as a result of holding the crystal briefly at 110 K. They have distorted shapes, one pointing upward near 3245 G and the other pointing downward near 3390 G, and they likely arise from a single

defect. Since their integrated intensity (i.e., concentration) is considerably less than that of the broad trapped-hole center, we will not include these two lines in our discussion. A very unusual EPR ''feature'' was also observed. Instead of having a normal derivative shape, it only drops below the baseline with a minimum occurring near 4400 G. This feature is part of a broader EPR signal that was initially observed in Mg-doped stoichiometric $LiNbO_3$ by Sweeney *et al.* The entire spectrum extends from 2900 to 4400 G when the magnetic field is along the *c* axis, and was referred to as a ''new electron trap'' by these investigators. This broad EPR spectrum also has been observed by Zaritskii, Rakitina, and Polgar and referred to as a ''thermal defect.'' Based on these two investigations, the presently accepted model of the center responsible for this unique spectrum is an electron trapped at a regular niobium site (i.e., a Nb_{Nb}^{4+}) with perhaps a Mg_{Li}^{2+} ion nearby. Note that this center also gives rise to the 1200-nm absorption band. In the remainder of this paper, we refer to this center as the ''shallow-trapped electron,'' and view it to a first approximation as a self-trapped electron while at the same time acknowledging that a Mg^{2+} ion may be in the near vicinity. After the crystal was warmed to 110 K and then returned to 20 K, the EPR feature associated with the shallow-trapped electron is no longer present.

Our investigation focused on 1% Mg stoichiometric $LiNbO_3$ crystals. These crystals differ from the more widely studied congruent $LiNbO_3$ crystals in one major respect. In congruently grown crystals, niobium ions occupy lithium sites and thus provide charge compensation for the large numbers of lithium vacancies that are present. In the 1% Mg stoichiometric crystals, there are very few niobium ions on lithium sites and instead, the divalent magnesium ions on lithium sites provide charge compensation for the smaller number of lithium vacancies that are present. Overall, the concentrations of point defects are considerably less in 1% Mg stoichiometric crystals compared to congruent crystals. This is reflected in the stoichiometric crystals by narrower EPR lines in the spectra of transition-metal-ion impurities such as Fe^{3+} (i.e., linewidths are reduced as the random strain in the crystal is removed). The ability to detect emitted light from the 1% Mg stoichiometric crystals directly correlates with the lack of niobium antisite defects. A bright blue (440 nm) thermoluminescence peak at 94 K was easily observed in the case of the Mg-doped stoichiometric crystals, while similar experiments on congruent $LiNbO_3$ crystals gave no observable TL results.

There are two primary goals in an investigation of a TL peak. These are, first, to identify the participating electron and hole traps and, second, to determine the recombination site (in other words, does the electron move to the hole or does the hole move to the electron). We have used both optical absorption and EPR to obtain information about the electron and hole traps participating in the 94-K TL peak. Our EPR results suggest that the usual trapped hole center, reported by earlier investigators, is produced in a 1% Mg stoichiometric crystal at 77 K by the x rays and ultraviolet lasers. We base this assignment on the observed linewidth of 150 G and the

g value of 2.03 (see Fig. 6(a)). The model for this holelike center, although not absolutely established in the literature, is commonly accepted to be a hole trapped on an oxygen ion adjacent to a lithium vacancy. Our EPR and optical absorption results suggest that a shallow electron center, reported by earlier investigators, is produced in a 1% Mg stoichiometric crystal at 77 K by the x rays and ultraviolet lasers. This assignment is based on the presence of the 1200-nm absorption band and the broad-downward EPR feature near 4400 G. The model for this shallow electron center is an electron trapped on a regular niobium with perhaps a Mg^{2+} ion nearby. We note that these shallow electron centers are not readily formed in congruent $LiNbO_3$ crystals because of the presence of a very large concentration of niobium antisite defects (Nb_{Li}^{5+}). These antisite ions are closely spaced on average in the congruent crystals. Thus, if a niobium antisite defect is nearby, an electron will not remain localized on a regular niobium but will move the several lattice spaces to the deeper niobium antisite trap (because of the strong electrostatic attraction exerted by the highly charged antisite defect). The decreased probability of stabilizing a significant number of isolated shallow electron centers explains why the intensity of the blue emission is usually much smaller in congruent $LiNbO_3$ crystals.

The warming step to 110 K provides information about the mechanisms responsible for the observed thermoluminescence peak. When the temperature of the irradiated crystal was increased to 110 K (i.e., when replicating the TL experiment), approximately 60% of the hole centers disappeared and 100% of the shallow electron centers disappeared. These results suggest that the TL peak at 94 K is produced when the trapped electrons become unstable and move to the trapped hole centers. More specifically, the center that disappears completely is the center that becomes unstable and moves. Thus, we suggest that the radiative recombination occurs at or very near the hole site. Early investigators proposed that laser- and x-ray-induced luminescence from undoped $LiNbO_3$ crystals was a result of recombination at regular NbO_6 units, and our present thermoluminescence data are not in significant disagreement with this suggestion. We envision the recombination process to occur as follows. The shallow electron centers become thermally unstable near 94 K, the released electrons then move from niobium to niobium until they reach a niobium next to the oxygen with the trapped hole, and finally the hole and the electron recombine. In our model, the re-combination takes place within an NbO_6 unit containing the oxygen ion where the hole was initially trapped. This is not a regular NbO_6 unit, but one that is slightly perturbed by a neighboring lithium vacancy (i.e., the lithium vacancy that initially stabilized the hole). When visualizing our recombination model, it is important to recall that each oxygen ion in the $LiNbO_3$ lattice has four cation neighbors, two lithiums and two niobiums.

A final point refers to the mechanisms involved in initially producing the trapped holes and trapped electrons that contribute to the 94-K TL peak. A direct band-to-band ionization

process is expected in the case of the 60-kV x rays. In contrast, we note that our laser wavelengths (325 and 355 nm) are well below the fundamental band edge of the crystal at 77 K. For photons at these wavelengths to form separated electrons and holes (that can recombine on warming), we suggest that the broad charge-transfer absorption band of the Fe^{3+} ions, peaking near 320 nm, must be involved. The precise mechanism is unknown, but we can envision the following scenario. Absorption of a photon in the charge-transfer band will result in the transient formation of an Fe^{2+} and an adjacent O^- ion, as an electron is transferred temporarily from the oxygen to the iron. This electron and hole may simply recombine nonradiatively at the original Fe–O site and restore the original charge configuration. It is also possible that the electron and the hole will separate (since the newly formed Fe^{2+} and the hole both have an effective positive charge relative to the regular lattice). This electrostatic repulsion force on the hole may cause it to move away from the Fe^{2+}, and thus become free to migrate through the lattice until it finds a stabilizing entity such as lithium vacancy. A second photon could then ''move'' the electron away from the remaining Fe^{2+} ion. This would occur in the same way that photorefractive gratings are written in Fe-doped $LiNbO_3$ crystals (i.e., electrons are ''moved,'' in an intervalence transfer, from Fe^{2+} ions to a neighboring niobium ion by wavelengths that fall within the very broad 490-nm optical absorption band associated with the Fe^{2+} ions). This absorption of the second photon by the Fe^{2+} ion restores the initial Fe^{3+} ion and, at the same time, forms a shallow-trapped electron center at one of the regular niobium sites well removed from the initial Fe^{3+} ion. Although this scenario to produce separated electrons and holes with below-band-gap light involves the sequential absorption of two photons, the corresponding formation rate is expected to depend linearly on light intensity. A linear dependence results from the long lifetimes, at 77 K, of the trapped hole and the Fe^{2+} ion formed in the first stage of the process. There may be other variations of the scenario we have just described that involve a more direct transfer of an electron into the conduction band by below-band-gap light. In particular, it is possible that the absorption of a photon in the charge-transfer band of the Fe^{3+} ions results in the transient formation of an Fe^{2+} (in its excited state), with an adjacent O^- ion, and that thermal energy then moves the excited-state electron from the iron to the conduction band. This leaves the hole on the oxygen free to migrate away to a trapping entity such as a lithium vacancy.

IV. Results from $LiTaO_3$

The $LiTaO_3$ crystals used in the present investigation were obtained from Yamaju Ceramics (Japan). As-received, these were congruently grown optical grade samples in the form of c plates with dimensions of 10 x 10 x 1 mm^3. Several samples were given a post-growth vapor-transport-equilibration (VTE) treatment at Stanford University. In this procedure, the congruent $LiTaO_3$ wafer is placed in a platinum crucible over a mixture of Li_3TaO_4 and $LiTaO_3$ polycrystalline powder with a surrounding static atmosphere of dry O_2 or N_2. The crucible and

sample are then held near 1360°C for approximately 200 h. Lithium ions diffuse into the crystal during this treatment and eliminate nearly all of the lithium vacancies and their corresponding tantalum antisite charge compensators (Ta_{Li}) that had formed during the initial congruent growth. The resulting composition is very nearly stoichiometric after a VTE treatment, i.e., the [Li]/[Ta] ratio is greater than 0.99. Small samples with dimensions of 10 x 3 x 1 mm^3 were cut from the congruent and VTE-treated crystals for use in the TSL, EPR, and optical absorption experiments.

Optical absorption spectra from a VTE-treated $LiTaO_3$ crystal are shown in Fig. 5. These data were taken at room temperature and at 77 K using unpolarized light propagating along the c axis, and they show the shift in the band edge from 262 nm to 248 nm as the temperature is lowered. There is a near-edge absorption band in these spectra that is attributed to a charge-transfer transition of Fe^{3+} ions (i.e., a transition in which an electron moves from an adjacent oxygen ion to the Fe ion). It peaks at approximately 300 nm and does not shift appreciably as the temperature is lowered. A possible second charge transfer band, associated with Fe^{3+} or another transition-metal-ion impurity is emerging near 255 nm in the absorption spectrum taken at 77 K. Our VTE-treated $LiTaO_3$ crystals exhibited sharp EPR lines from trace levels of Fe^{3+} and Co^{2+} impurity ions.

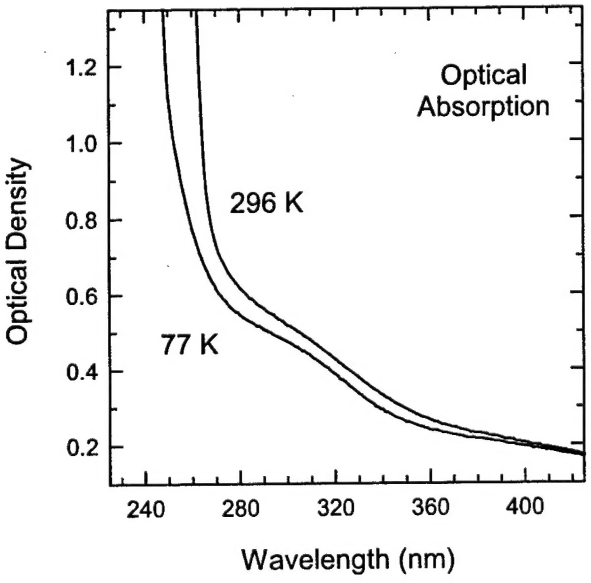

Figure 5. Optical absorption from a VTE-treated $LiTaO_3$ crystal. These data were taken at room temperature and at 77 K with unpolarized light propagating along the c axis. The absorption band near 300 nm is attributed to trace amounts of Fe^{3+} ions.

Thermally stimulated luminescence results from a VTE-treated $LiTaO_3$ crystal are shown in Fig. 6. These data are presented in a three-dimensional plot with temperature, wavelength, and intensity as the axes. Prior to the warming depicted in Fig. 6, the sample was exposed to the pulsed 355-nm laser beam while being held at 77 K. Then, a rapid increase in temperature

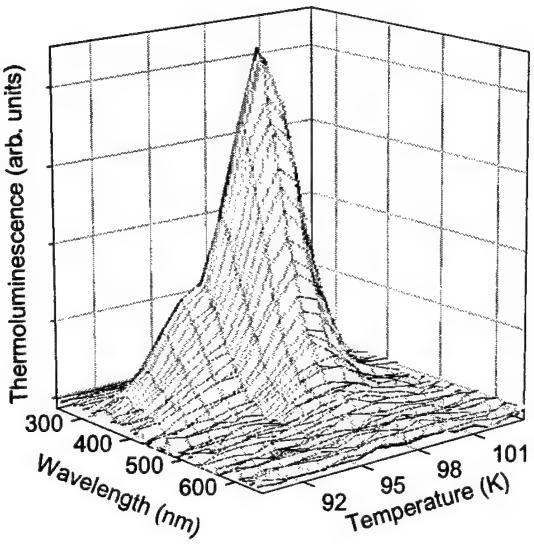

Figure 6. Three-dimensional view of the TSL data from a VTE-treated $LiTaO_3$ crystal that had been irradiated at 77 K with a pulsed 355-nm laser. The intensity of the emission is plotted as a function of both temperature and wavelength.

produced the TSL. The rate of heating was approximately 9.6 K/s, and this allowed the spectrograph and CCD camera to obtain a complete wavelength dependence of the emission every 1.0 K. Figs. 7 and 8 contain cross-sectional views of the data in Fig. 6. The temperature dependence, shown in Fig. 7, was measured at the wavelength corresponding to the peak of the emission. There are two very closely spaced peaks in this TSL spectrum, a weaker emission near 94 K and a more intense peak near 98 K. We repeated this experiment numerous times to verify the existence of both TSL peaks. The wavelength dependence shown in Fig. 8 represents the emission observed at 98 K (the same wavelength dependence also was observed at 94 K). These

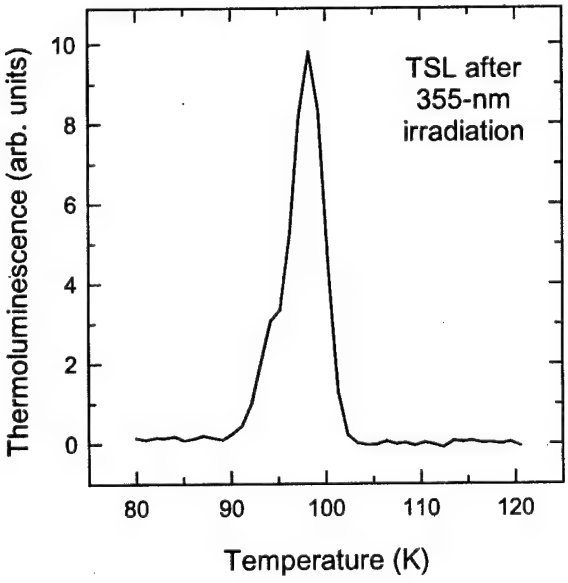

Figure 7. A cross-section view (taken from Fig. 6) showing the temperature dependence of the TSL from a VTE-treated $LiTaO_3$ crystal. These data correspond to a wavelength of 350 nm (i.e., the maximum in the emission). Two overlapping TSL peaks are observed, one near 94 K and one near 98 K.

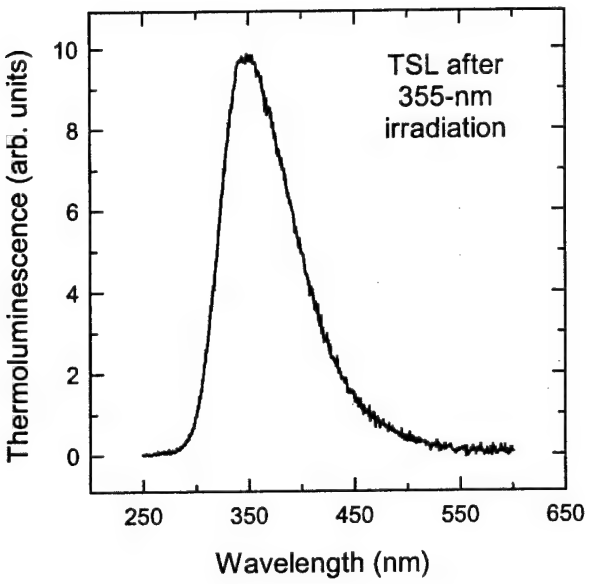

Figure 8. A cross-section view (taken from Fig. 6) showing the wavelength dependence of the TSL from a VTE-treated $LiTaO_3$ crystal. These data correspond to a temperature of 98 K (i.e., a maximum of the emission). The TSL peak occurs near 350 nm.

data in Fig. 8 have been corrected for system response, and they show that the peak in the emission occurs near 350 nm. In addition to the pulsed 355-nm laser beam, three other excitation sources (60-kV x rays, a pulsed 266-nm laser beam, and a cw 325-nm laser beam) were also used to produce the TSL in the VTE-treated $LiTaO_3$ crystals. The results obtained using these latter excitation sources were identical to the results shown in Figs. 6, 7, and 8. In contrast, we did not observe any emission from our congruent $LiTaO_3$ crystals, even though the same experimental procedures were followed and the same excitation sources were used.

Separate optical absorption and EPR experiments were performed to help identify the electron and hole centers contributing to the TSL peaks in Fig. 6. Optical absorption data in the near infrared were obtained at 10 K before and during the exposure of a VTE-treated $LiTaO_3$ crystal to a 325-nm laser beam. This ultraviolet laser excitation produced a broad absorption band peaking near 1600 nm, as shown in Fig. 9. The curve presented in Fig. 9 is a "difference" spectrum (i.e., absorption data taken before the crystal was exposed to the laser have been subtracted from absorption data taken while the crystal was exposed to the laser). This 1600-nm absorption band, optically induced at low temperature, has not been previously reported in $LiTaO_3$ crystals. When considering an assignment for this band, we note its similarity to the infrared absorption band peaking near 1200 nm in stoichiometric $LiNbO_3$ crystals. In this latter material, the infrared absorption band is attributed to a shallow electron trap, i.e., an electron trapped on a regular substitutional niobium ion. By analogy, we suggest that the 1600-nm absorption band formed at low temperature in VTE-treated $LiTaO_3$ is also a shallow electron trap, with the electron localized on a regular substitutional tantalum ion (i.e., a Ta_{Ta}^{4+} center). Unfortunately, this 1600-nm absorption band is sensitive to infrared bleaching light and is easily

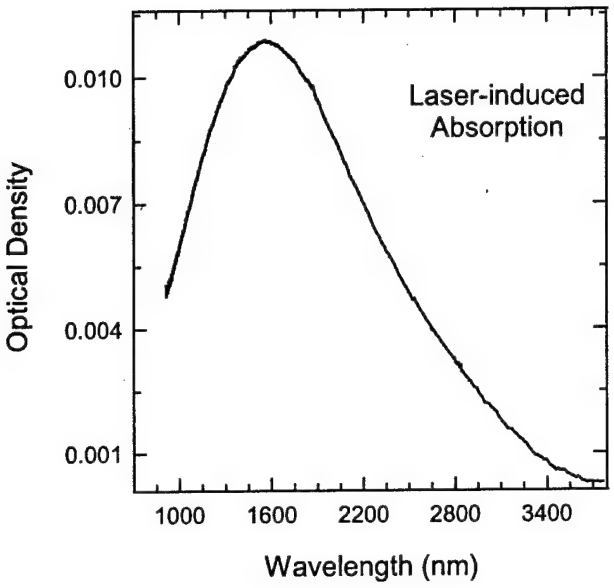

Figure 9. Optical absorption from the shallow electron trap, produced at 10 K by a 325-nm laser beam. This 1600-nm absorption band was obtained by subtracting the spectrum taken before exposure to the laser from the spectrum taken during exposure to the laser.

destroyed optically when experiments to determine its thermal stability, such as repeated absorption scans at various low temperatures, are attempted.

The series of low-temperature EPR spectra shown in Fig. 10 were obtained from a VTE-treated $LiTaO_3$ crystal. These data were taken at 40 K with the magnetic field parallel to the c axis. Trace (a) in Fig. 10 is from the as-treated crystal, prior to irradiation. The more intense EPR signal located near 3380 G is one of several lines associated with the Fe^{3+} ions that substitute for Li^+ ions. The crystal then was irradiated at 77 K with x rays and rapidly transferred into the cold helium gas ($\approx$ 40 K) flowing through the microwave cavity. Trace (b) was taken after the irradiation, but before an annealing step. The Fe^{3+} signal has decreased significantly (by a factor of more than three) as a result of the 77-K irradiation, and a three-line spectrum has appeared. This latter spectrum has been reported in several earlier studies and is assigned to a hole center, where the hole is either self-trapped on one or more oxygen ions in an otherwise perfect region of the crystal or trapped on an oxygen ion next to a lithium vacancy. Next, the conditions that produced the TSL peaks at 94 K and 98 K (see Fig. 7) were replicated by warming the irradiated crystal to 100 K while in the microwave cavity, holding it there for 5 min, and then finally returning to 40 K where the spectrum in trace (c) of Fig. 10 was taken (with the same spectrometer settings and the same orientation of magnetic field). This 100-K anneal removed the three-line trapped hole center and increased the concentration of Fe^{3+} ions by approximately 50%. At the same time, a new four-line hole center has emerged, as illustrated by the lower stick diagram for trace (c) in Fig. 10. This four-line EPR spectrum has not been previously reported. Finally, in a second and final anneal, the sample was warmed to 130 K while in the microwave cavity, held for 5 min, and then returned to 40 K where the spectrum in

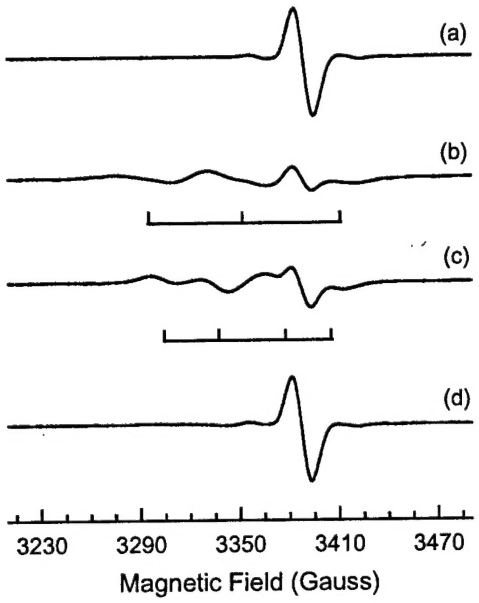

Figure 10. EPR spectra from a VTE-treated $LiTaO_3$ crystal taken (a) before irradiation, (b) after exposure to x rays at 77 K, (c) after a five-min anneal at 100 K, and (d) after a five-min anneal at 130 K. The measurement temperature was 40 K and the magnetic field was parallel to the c axis.

trace (d) of Fig. 10 was taken. During this anneal, the four-line hole center disappeared completely and the concentration of Fe^{3+} ions returned to the pre-irradiation value, as shown by comparing trace (d) with trace (a). Similar EPR results, although with lower signal-to-noise ratios, were observed when a VTE-treated $LiTaO_3$ crystal was initially exposed to a 325-nm laser beam while being held in the microwave cavity at temperatures below 77 K. Experiments were not performed to determine if the 266 and 355 nm laser beams would produce these EPR results since it was difficult for us to transfer these beams to the microwave cavity.

The thermally stimulated luminescence described in this paper has only been observed in undoped $LiTaO_3$ crystals that were congruently grown and then VTE-treated. When a crystal was cut from the same congruently grown boule, but not VTE-treated, then the emission was not seen. It is generally known (in analogy with $LiNbO_3$) that congruently grown $LiTaO_3$ crystals contain large numbers of lithium vacancies, with charge compensation provided by tantalum antisite defects (i.e., tantalum ions substituting for lithium ions). During the post-growth VTE treatment, lithium ions enter the crystal and eliminate nearly all of these lithium vacancies. The tantalum ions that initially occupied lithium sites are then no longer needed for charge compensation and they diffuse to the surface of the crystal. This process leaves the $LiTaO_3$ crystal in a form that is very nearly stoichiometric. We suggest that the occurrence of radiative recombination (i.e., emission of light when electrons and holes recombine) at low temperatures in the VTE-treated $LiTaO_3$ crystals directly correlates with the removal of these lithium vacancies and the tantalum antisite defects. Removal of the tantalum antisite defects is

especially important because they were providing an efficient nonradiative recombination site for electrons and hole in the congruent $LiTaO_3$ crystals.

Our EPR and optical absorption data provide information about the electron and hole traps that contribute to the TSL peaks observed between 90 and 100 K in $LiTaO_3$. Referring to Fig. 10, we see in trace (b) that an irradiation at 77 K with x rays produces a "three-line" EPR spectrum representing a trapped-hole center and also decreases the intensity of the Fe^{3+} EPR line (indicating that the Fe^{3+} ions trap an electron and become Fe^{2+} ions). In addition, our optical absorption results in Fig. 9 show that ionizing radiation at low temperature forms a shallow electron center when an electron is trapped on a regular tantalum ion (i.e., the Ta_{Ta}^{4+} center). This suggests that one hole center and two electron centers are formed during the 77-K irradiation, and that the number of hole centers produced is equal to the combined number of electron centers.

Next, we consider the behavior of these defects when the crystal is warmed to 100 K, an annealing step that duplicates the conditions that caused the TSL peaks. Trace (c) in Fig. 10 shows that the three-line hole center is no longer observable and the Fe^{3+} has only partially recovered. This suggests that the three-line trapped-hole centers become thermally unstable below 100 K, thus allowing these holes to migrate to other defects. There are three destinations for these holes. Some of the holes will move to Ta_{Ta}^{4+} defects and others will move to Fe^{2+} ions, recombining with the trapped electrons in each case. At the same time, a portion of the holes will move to "deeper" trapping sites in the crystal and form a new more stable hole center. Verification that the latter two cases occur is provided by trace (c) in Fig. 10 when the Fe^{3+} signal partially recovers and a new four-line hole center appears. We expect that recombination at the Ta_{Ta}^{4+} centers will be radiative, and that recombination at the Fe^{2+} ions will be nonradiative.

From this analysis, we conclude that the primary mechanism leading to the observed TSL peaks in $LiTaO_3$ is the release of holes from the three-line center and their recombination with electrons that had been "self-trapped" in the form of Ta_{Ta}^{4+} centers. The appearance of the two TSL peaks, at 94 and 98 K, may result from one of the two following possibilities. First, the three-line hole center has relatively broad EPR lines and could represent two very similar, yet distinct, hole centers that would thermally release their holes at slightly different temperatures. Second, we do not know the decay temperature for the shallow tantalum electron center, but we believe it also may be in the mid-90 K region, by analogy with $LiNbO_3$. If this is the case, then within a small temperature range, we would have holes moving to recombine at sites where electrons are trapped and also electrons moving to recombine at sites where holes are trapped (i.e., both the three-line hole centers and the Ta_{Ta}^{4+} centers may be radiative recombination

sites). In each event, the recombination would take place in TaO_6 units, and would agree with the observation that the 94 and 98 K TSL peaks have the same spectral output, peaking near 350 nm.

Although reported in earlier studies, a definitive model has not yet been established for the hole center represented by the three-line EPR spectrum in trace (b) of Fig. 10. Plausible models in which the hole is localized on an oxygen ion, either self-trapped as a result of lattice relaxation or stabilized by an adjacent entity such as a lithium vacancy, were suggested in the previous section. Because the three lines in the c-axis EPR spectrum have 1:2:1 intensity ratios, it was initially thought that equal hyperfine interactions with two 100% abundant I = 1/2 nuclei such as hydrogen were responsible for the structure. However, the work of Gonzalez et al. has cast considerable doubt on that possibility. We also note that at the present time there is no definitive model for the hole center represented by the four-line EPR spectrum in trace (c) of Fig. 10.

V. EPR of Fe^{3+} Impurities in $LiTaO_3$

In photorefractive oxides, Fe^{3+} ions play a central role in the charge transfer and trapping processes. Usually, the EPR spectra of the Fe^{3+} ions consists of extremely broad lines and gives very little information. Fortunately, the VTE-treated $LiTaO_3$ crystal exhibited narrow EPR lines and was ideal for a careful study of the Fe^{3+} ions. This effect is shown in Figure 11.

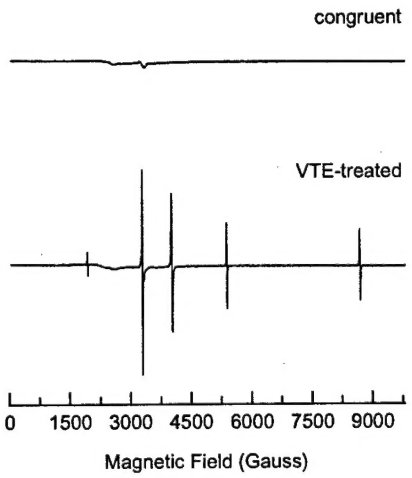

Fig. 11. Comparison of EPR spectra from $LiTaO_3$. The top trace is from a congruent crystal and the bottom trace is from a VTE-treated crystal.

Because of the sharp Fe^{3+} lines in our VTE-treated $LiTaO_3$ crystal, we were able to rigorously investigate its ground state angular dependence. These results are shown in Figure 12 where the magnetic field is rotated in 5° intervals from the c axis to the a axis.

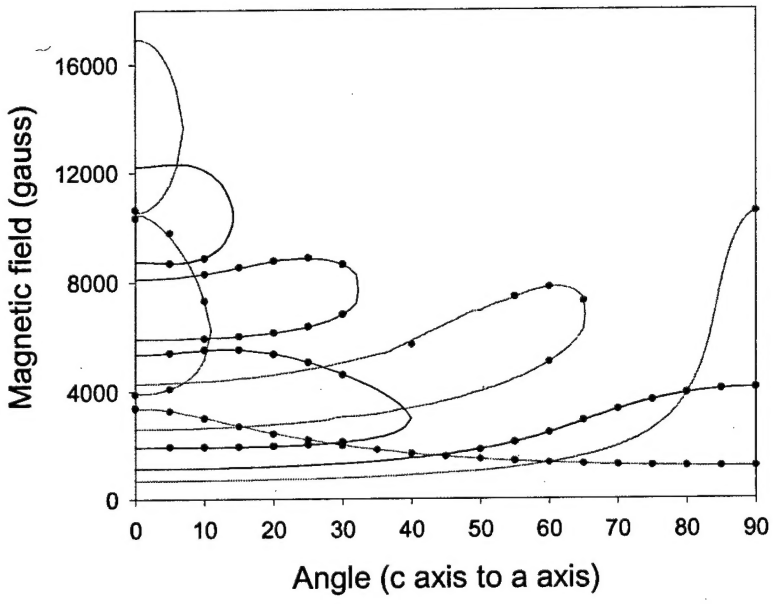

Fig. 12. Angular dependence of the EPR spectrum of the Fe^{3+} ion in $LiTaO_3$.

The following spin-Hamiltonian was used to extract g matrix and crystal-field parameters from the angular dependence shown in Figure 12. The first term on the right is the electron Zeeman, the second term is the 2nd order crystal field, and the third term is the 4th order crystal field.

$$H = \beta \mathbf{H} \cdot \mathbf{g} \cdot \mathbf{S} + \sum_{q=-2}^{2} B_2^q O_2^q + \sum_{q=-4}^{4} B_4^q O_4^q$$